INSTITUTE OF PHYSICS PUBLISHING JOURNAL OF PHYSICS D: APPLIED PHYSICS
J. Phys. D: Appl. Phys. **38** (2005) A61–A66 doi:10.1088/0022-3727/38/10A/012

Goniometric and topographic characterization of synthetic IIa diamonds

Kenji Tamasaku, Tomoyasu Ueda, Daigo Miwa and Tetsuya Ishikawa

SPring-8/RIKEN, Mikazuki, Hyogo 679-5148, Japan

Received 1 March 2005
Published 6 May 2005
Online at stacks.iop.org/JPhysD/38/A61

Abstract
Synthetic type IIa diamonds were characterized using rocking curve measurements and x-ray topography with quasi-plane-wave incidence, and high resolution reciprocal space mapping. The rocking curves of the (111) crystals were comparable to the theoretical ones. Some crystals had wider rocking curves because of the higher density of stacking faults. Even the highest quality crystal did not give the theoretical rocking curve due to dislocations and strain bands. On the other hand, the (100) crystals had nearly perfect area. The difference was attributed to the orientation of the seed crystal.

(Some figures in this article are in colour only in the electronic version)

1. Introduction

Diamonds have been expected to be good candidates for optical elements in synchrotron radiation science because of their superior thermal and optical properties, i.e. low linear thermal expansion coefficient, high thermal conductivity and low x-ray absorption (Freund 1995). However, the utilization of diamonds has been limited to phase retarders and monochromators for branch beamlines. Most high-heat-load monochromators, e.g. 18 of 20 hard x-ray undulator beamlines in SPring-8, still are silicon rather than diamond, because the available quality and size of diamonds are believed to be insufficient.

The need for perfect diamonds may be more serious for forthcoming self-amplified spontaneous emission free-electron-lasers (SASE FEL), such as LCLS at SLAC (Arthur *et al* 2002), TESLA XFEL at DESY (Brinkmann *et al* 1997) and SCSS at SPring-8 (Shintake 2004), which will deliver FEL pulses with huge peak powers of several gigawatts. Although the average power is much lower than the third generation sources and is easily manageable, the peak energy dose to the first crystal of the monochromator is close to the melt limit for most materials; e.g. the melt limit of silicon is estimated to be 0.4 eV atom^{-1} (Arthur *et al* 2002, chap. 9) and the peak energy dose is calculated to be 0.1 eV atom^{-1} for 6 keV FEL beam at SCSS. Only low-Z materials, such as Li, Be, B and C, can be used owing to lower photo-ionization cross sections. Considering preservation of high spatial coherence of the FEL beam, perfect diamonds should be the unique solution.

In this context, we characterized high quality synthetic type IIa diamonds, which have become available recently. We focused on the diffraction property and its relation to defects.

2. Experimental

We prepared four (111) and eleven (100) synthetic type IIa diamonds grown by Sumitomo Electric Industries Ltd using a high-pressure high-temperature technique (Toda *et al* 1997). The surface of (111) crystals were as-cleaved, because polishing of the (111) surface required an offset angle of about 1°, which would make the analysis complicated. The surface of (100) crystals were lapped without offset. The surface profile was measured by a scanning white light interferometer (Zygo New View, Zygo). These crystals were characterized using rocking curve measurements, x-ray topography and reciprocal space mapping. We used a non-dispersive parallel set-up for higher angular resolution, i.e. collimator and analyser crystals that had d spacings close to the netplanes of diamonds. Table 1 summarizes the netplanes of the collimator and

Table 1. Summary of the netplanes of the collimator and the analyser and the relevant parameters.

Diamond	Collimator/analyser	$\Delta d/d$	Energy (keV)
(111)	Si(220)	0.073	9.44
(400)	Si(531)	0.029	19.75
(220)	Si(331)	0.012	14.55

the analyser and the relevant parameters. The x-ray measurements were performed at the RIKEN coherent x-ray physics beamline (BL29XU) of SPring-8 (Tamasaku *et al* 2001).

Both the rocking curve measurements and x-ray topography were performed at the 1 km station so as to use a large area and a highly parallel x-ray beam. The angular divergence was less than 0.6 μrad (full width at half maximum, FWHM). In addition, the collimators were cut asymmetrically with an asymmetric factor of 20.9 for quasi-plane-wave incidence with a divergence of 0.03 μrad. In this set-up the rocking curve nearly agreed with the intrinsic rocking curve, and x-ray topography became quite sensitive to strain (Ishikawa 1990).

The rocking curve was measured using the whole surface and a selected area with a beam size of 0.5×0.5 mm^2. We chose a nearly defect-free area for the smaller beam size monitoring the reflected beam image.

The topograph was measured using a CCD-based beam monitor (Hamamatsu, AA-20MOD) with a pixel size of $12 \times 12\,\mu$m^2. To analyse the positional dependence of the rocking curve, the reflected beam images were recorded with $0.5''$ steps for the 111 reflection and $0.15''$ for the 400 reflection. The local width of the rocking curve and the local Bragg angle were extracted for each CCD pixel from the reconstructed local rocking curve using the beam images (Lübbert *et al* 2000).

The reciprocal space maps were measured at the first station of BL29XUL. We used a triple crystal set-up with four-bounce symmetric channel-cut crystals as the collimator and the analyser (table 1) for higher reciprocal space resolution (Iida and Kohra 1979). The collimator, the sample and the analyser were set non-dispersively. The 111 reciprocal space point was measured within the [111]–[$2\bar{1}\bar{1}$] and the [111]–[$01\bar{1}$] planes for the (111) crystals, and the 400 reciprocal space point within the [100]–[011] and the [100]–[$0\bar{1}1$] planes for the (100) crystals. Several points on the surface were measured with a beam size of 0.5×0.5 mm^2 to check positional dependence.

3. (111) crystal

Figure 1 shows rocking curves of sample 1 ($8 \times 5.5 \times 0.7$ mm^3) and 2 ($10 \times 5 \times 0.7$ mm^3), which were selected as the typical (111) crystals, with the 111 reflection in the reflection geometry, together with the theoretical curve calculated using the DuMond diagram (Nakayama *et al* 1973). Both the rocking curves had narrow widths comparable to the theoretical ones, indicating higher quality. When the beam size became smaller, the rocking curve became closer to the theoretical one. The width was $4.75''$ in the FWHM, whereas the theoretical width was $4.4''$. Although the rocking curves were comparable to the theoretical ones, we observed a sample dependence of the width.

When we compared quasi-plane-wave topographs, sample 1 (figure 2(*a*)) was found to include more defects, especially stacking faults, than sample 2 (figure 2(*b*)). The width of the rocking curve seems to be related to the density of the defects.

To elucidate the relation between the density of stacking faults and the width of the rocking curve, we measured reciprocal space maps of both the crystals. The 111 reciprocal space point of sample 1 did not spread uniformly, but was

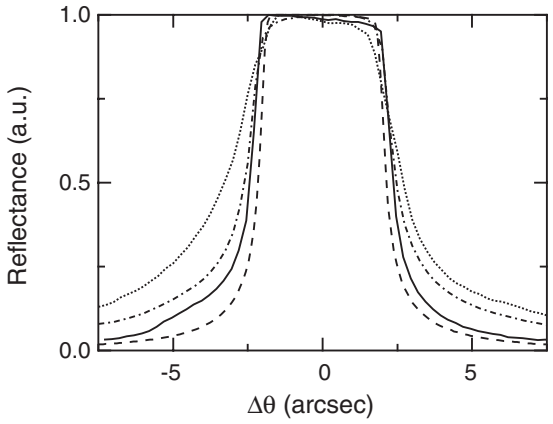

Figure 1. Rocking curves of the 111 reflection in the reflection geometry. Sample 1 (· · · · · ·) and 2 (— · —) measured on the whole surface. Sample 1 (——) with the selected area. The dashed line indicates the theoretical curve.

characterized by two strong streaks (figure 3(*a*)). These streaks broaden the rocking curve, because the rocking curve corresponds to integrated intensities along the direction of the analyser streak as a function of Δq_x (Bowen and Tanner 1998). The streaks were found to be directed towards the projections of ⟨111⟩ directions from a geometrical consideration. The streak denoted as S1 was directed towards the [100] direction (the projection of [$1\bar{1}1$] and [$11\bar{1}$] directions), S2 towards [$\bar{1}11$], S3 towards [$14\bar{2}$] (the projection of [$11\bar{1}$]) and S4 towards [$1\bar{2}4$] (the projection of [$1\bar{1}1$]), respectively.

There are two possibilities of the origin of the ⟨111⟩ streaks, i.e. rough surface or stacking faults. In the surface scenario, the ⟨111⟩ streaks were made by crystal truncation rod (CTR) scattering from the {111} surfaces except the (111) surface. Oblique planes, such as ($11\bar{1}$), might be introduced by cleavage. The other possibility is discontinuity of the lattice at {111} stacking faults, which may cause the ⟨111⟩ streaks similar to the CTR scattering (Andrews and Cowley 1985).

The reciprocal space maps of sample 2 also had streaks, but much weaker and without S4 (figure 3(*b*)). Furthermore, S3 showed an interference effect, indicating that two planes were involved. The measured region did not include higher order maxima; we observed up to fourth maxima for other crystals (figure 3(*d*)). The separation of the two planes was the reciprocal of the distance between the origin and the first maximum, which was 1.2 μm along the [$01\bar{1}$] direction. We concluded that the streaks originated from the stacking faults. We note that ⟨111⟩ streaks had been observed for a silicon crystal with {111} stacking faults by Lomov *et al* (1985), though the streaks were ignored.

The ⟨111⟩ streaks may be related to the spike topography of diamonds (Clackson and Moore 1989). The spikes were usually directed towards the ⟨100⟩ directions; however, there are some reports of the ⟨111⟩ spike (Moore *et al* 1993). We consider that stacking faults have roles similar to voidites and platelets of the spike topography.

Next, we investigate the sample 2 using x-ray topography. Nearly the whole surface reflected the beam at the Bragg peak (figure 2(*d*)). Lines with low reflectance corresponded to surface scratches observed in the surface profile (figure 4(*a*)).

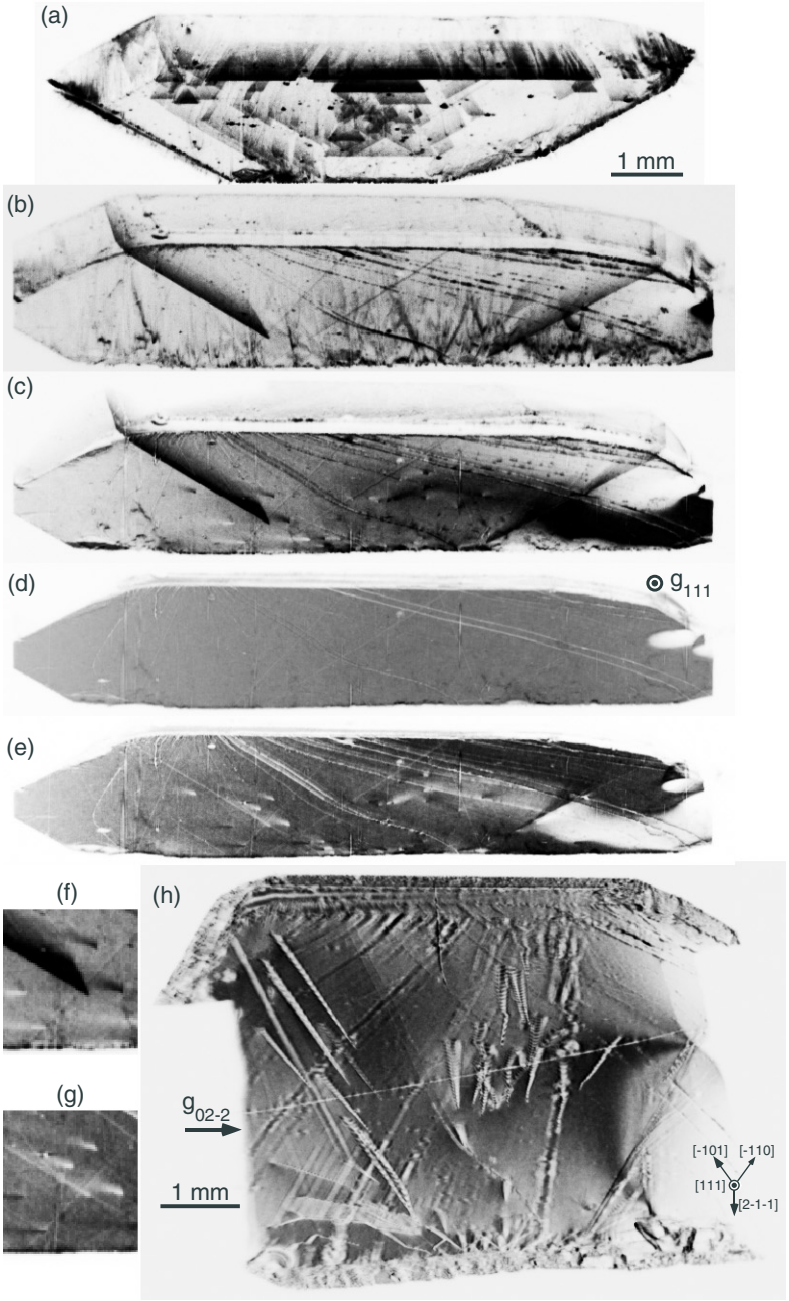

Figure 2. Reflection topographs (111 reflection) on the tail of the low angle side of the rocking curve of (*a*) sample 1 and (*b*) 2 and (*c*)–(*e*) sample 2 on the shoulder of the low angle side, the centre and the shoulder of the high angle side of the rocking curve. (*f*), (*g*) Magnified images of (*c*), (*e*). (*h*) Transmission topograph ($02\bar{2}$ reflection) of sample 2 on the centre of the rocking curve.

The low reflectance area on the right side was due to distortion.

In the topograph taken on the tail of the low angle side of the rocking curve (figure 2(*b*)), we observed two or three sets of stacking faults, outcrops of dislocations (black spots), and surface scratches (black lines). The stacking faults on the left side were inclined at 120° and the right side was 60° from the $[01\bar{1}]$ direction, so we considered the left as $(1\bar{1}1)$ and the right as $(11\bar{1})$ stacking faults. Note that the vertical scale is shrunk by a factor of about 0.32. Dark streaks extending from the lower part near the seed were not isolated defects, such as dislocations, but were considered as strain bands. We detected small amounts of Fe and Co around there by scanning fluorescent x-ray analysis (Tamasaku 2004). These impurities included in the early stage of crystal growth were considered as the origin of the dark streaks.

The surface scratches and the outcrops of dislocations were pronounced in the topographs on both shoulders of the rocking curve (figures 2(*c*) and (*e*)). Some outcrops had opposite contrast from the others (figures 2(*f*) and (*g*)), which was related to the sign of $\boldsymbol{g} \cdot \boldsymbol{b}$ where $\boldsymbol{g}$ is the diffraction vector and $\boldsymbol{b}$ is the Burgers vector.

Dislocations, some stacking faults, and surface scratches were clearly recognized in the transmission topograph (figure 2(*h*)). The dislocations extended radially from the lower centre part near the seed—in other words, perpendicular

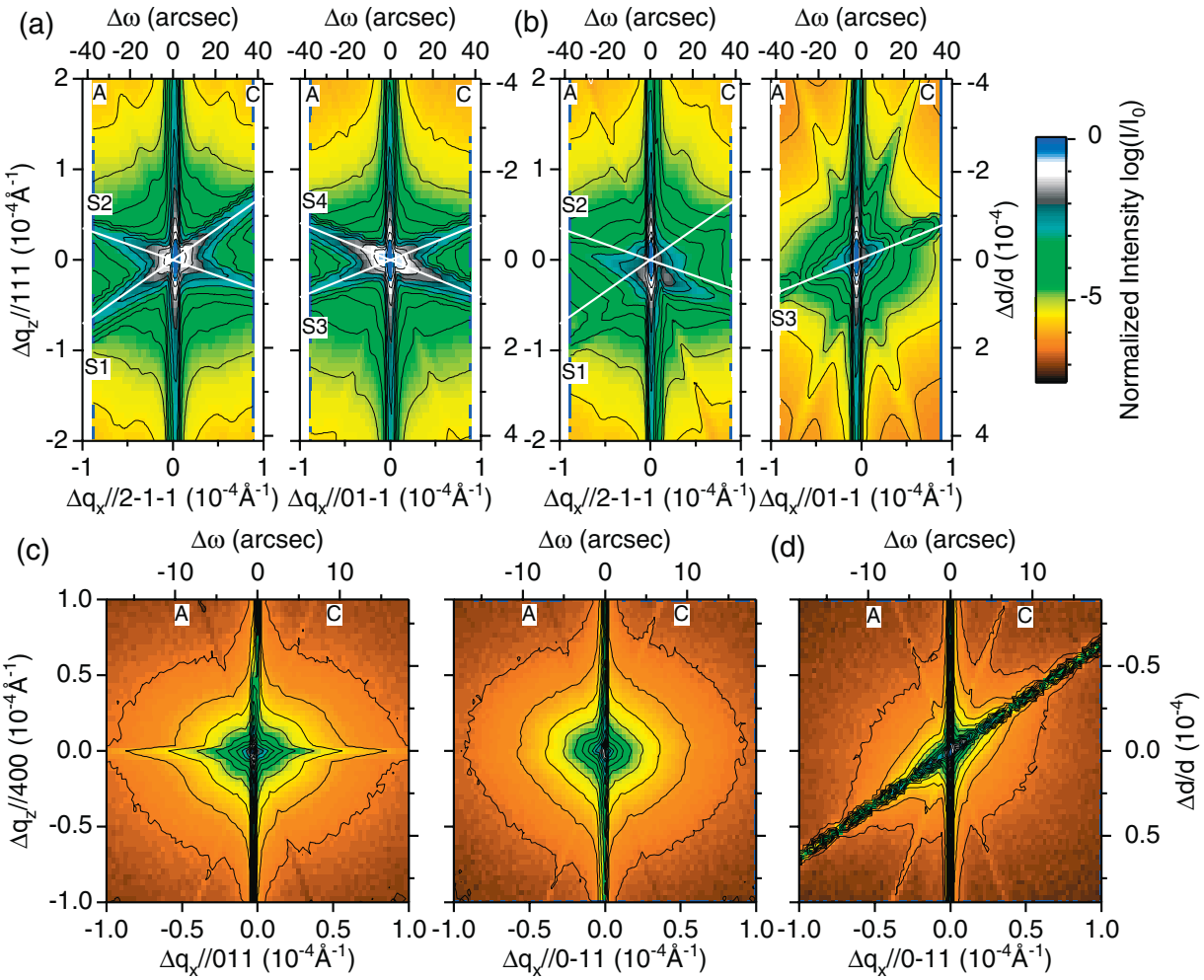

Figure 3. Reciprocal space maps of (*a*) sample 1 and (*b*) 2 around the 111 reciprocal space point within the [111]–[2$\bar{1}\bar{1}$] and [111]–[01$\bar{1}$] planes and of the (100) crystal around the 400 reciprocal space point (*c*) measured at the centre region of the surface within the [100]–[011] and [100]–[0$\bar{1}$1] planes and (*d*) measured on the peripheral region of the surface within the [100]–[0$\bar{1}$1] plane. C: collimator streak; A: analyser streak.

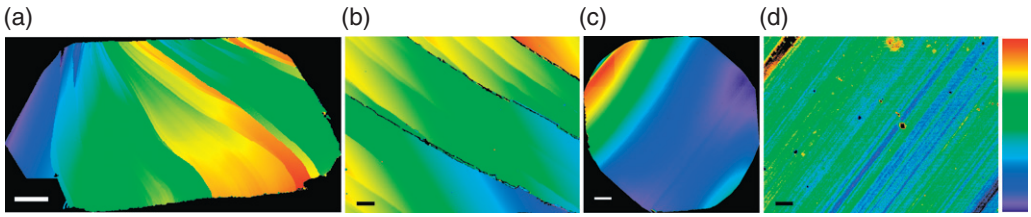

Figure 4. Surface profiles: (*a*), (*b*) the whole surface and the centre area of the sample 2 ((111) crystal). (*c*), (*d*) The whole surface and the centre area of the (100) crystal. (*e*) Full range of colour scale is 12.12 μm for (*a*), 1.94 μm for (*b*), 1.09 μm for (*c*) and 0.36 μm for (*d*). Horizontal bars correspond to 1 mm for (*a*), (*c*) and 10 μm for (*b*), (*d*).

to the growing faces. The observed surface scratches existed on the surface of beam entry because they became clearer due to dynamical effects.

As seen in figure 1 the flank of the rocking curve was very steep, i.e. about 0.5″. The sensitivity of the topographs taken at the flank is considered to be less than $\Delta\theta = 0.2''$ for a tilt of the lattice plane and less than $\delta d/d = \cot\theta_B \Delta\theta = 2.9 \times 10^{-6}$ for a change in the lattice constant, where θ_B is the Bragg angle. In the present measurements there was no evidence of growth sector nor growth banding, which had been observed in the x-ray topography of previous reports (Wierzchowski *et al* 1991, Kowalski *et al* 1996, Moore *et al* 1999, Hoszowska *et al* 2001). This is consistent with the low nitrogen concentration (less than 0.1 ppm) of type IIa diamonds (Toda *et al* 1997), which is a major reason for fluctuations in the lattice constant.

Figure 5(*a*) shows the positional dependence of the local Bragg angle. The local Bragg angle was nearly constant in the centre region of the surface, and there were no signs of bending of the lattice plane or a change in the lattice constant (Hoszowska *et al* 2001). The strain bands in the centre region and the surface scratches broaden the rocking curve (figure 5(*b*)). The local Bragg angle and the local width of

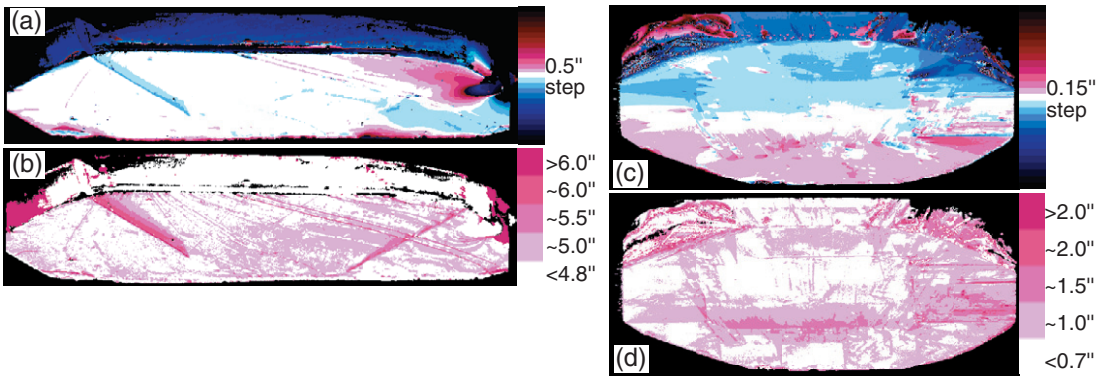

Figure 5. Positional dependence of (*a*) the width and (*b*) the centre of the rocking curve of sample 2 with the 111 reflection in the reflection geometry. (*c*) The width and (*d*) the centre for the (100) crystal with the 400 reflection in reflection geometry.

the rocking curve had strong positional dependence around the stacking faults and the distortion.

4. (100) crystal

We found most (100) crystals had narrow rocking curves compared to the theoretical calculation. An example of a (100) crystal ($10 \times 10 \times 0.7\,\mathrm{mm}^3$) is shown in figure 6. The rocking curve agreed with the theoretical one when we chose a defect-free area for the smaller beam size. The reason why the (100) crystals had higher quality than the (111) crystals was as follows. The (100) crystals were cut from the opposite side to the seed crystal but the (111) crystals contained the region near the seed, because the crystals were grown on the (100) seed crystals (Toda *et al* 1997).

We observed many outcrops of dislocations in the peripheral region in the reflection topograhs (figure 7(*b*)). Macroscopic bending of the lattice plane within the scattering plane was observed as reversed contrast between the flanks of the low and the high angle side of the rocking curve (figures 7(*a*) and (*c*)). The dislocations were clearly observed in the transmission topographs taken on the centre of the rocking curve (figure 7(*d*)) because of the dynamical effect, whereas the stacking faults became clearer at the tail on the low angle side (figure 7(*e*)) due to predominant direct images. The crystal had a large, rectangular, defect-free region at the centre, where the rocking curve agreed with the theoretical one. The difference in density of the defects seems to be related to the growth sector, i.e. the centre region was considered as the (100) growth sector and the most peripheral regions were the {111} growth sectors.

Traces of lapping were observed as oblique lines in the topographs (figures 7(*c*) and (*e*)). The lapped surface of the (100) crystals was smooth, as seen in figure 4(*c*), but had a microscopic wavy structure with a period of about 1 μm and a height of several tens of nanometres (figure 4(*d*)). The lines were directed towards the [010] direction, consistent with a previous report (Yarnitsky *et al* 1988).

The analysis of the quasi-plane-wave topographs shows clearly the bending of the lattice within the scattering plane, which is estimated to be about 0.3″ (figure 5(*c*)). Some crystals with wider rocking curves showed a larger bending of the lattice plane. The bending was considered to be due to residual

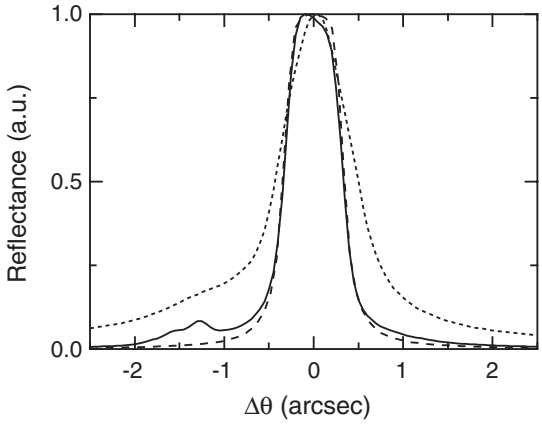

Figure 6. Rocking curves of the (100) crystal measured on the whole surface (· · · · · ·) and the selected area (——) with the 400 reflection in reflection geometry. The dashed line indicates the theoretical curve.

strain, and might be removed by annealing under a high-pressure, high-temperature condition. Figure 5(*d*) related the rocking curve width to defects, such as dislocations and the stacking faults observed in figure 7.

The bending of the lattice plane was found to be along the [011] direction from the reciprocal space mapping, which showed a horizontal streak only for the [100]–[011] map (figure 3(*c*)). No ⟨111⟩ streak was observed in the centre region of the surface. However, ⟨111⟩ streaks similar to the (111) crystals were observed on the peripheral region, and some of them showed the interference effect (figure 3(*d*)) whereas the other streaks were smooth (not shown).

5. Conclusion

Synthetic type IIa diamonds with sufficient quality for x-ray optics are now available, especially for the (100) crystals, when one selects crystals with lower stacking fault density and uses a nearly defect-free area. However, it is found that bending of the lattice plane caused a slight broadening of the rocking curve of some (100) crystals, and dislocations and strain bands broaden that of the highest quality (111) crystal. Further reduction of such defects is desired for use of diamonds at SASE FEL facilities. Crystal growth on the (111) seed crystals might be straightforward for perfect (111) crystals.

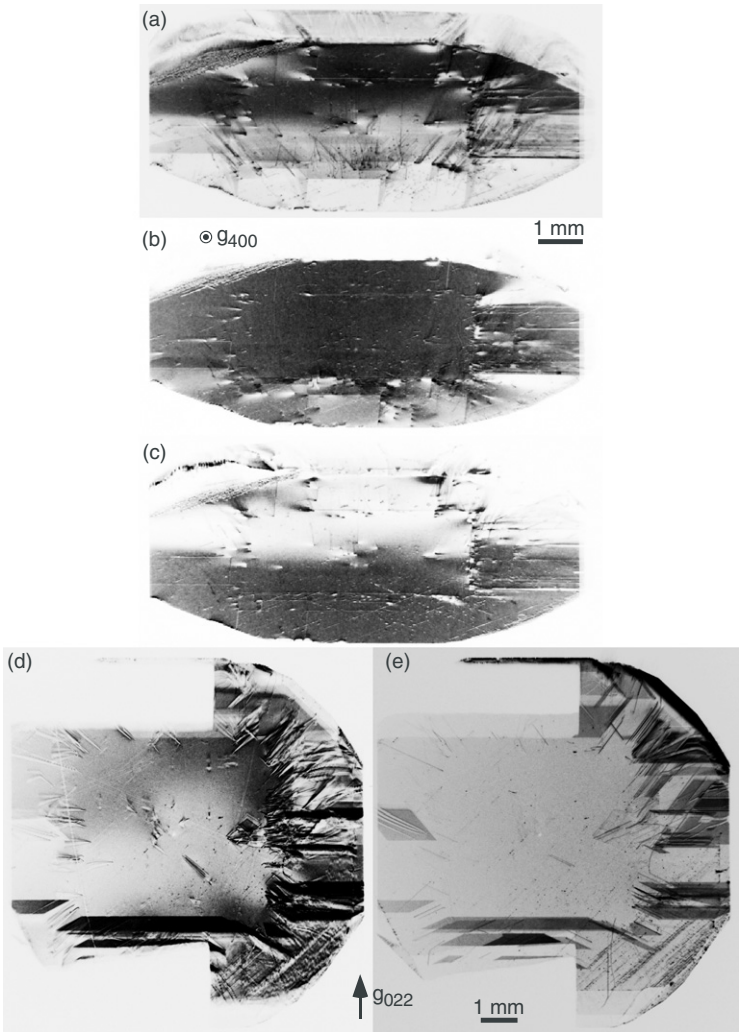

Figure 7. (*a*)–(*c*) Reflection topographs (400 reflection) of the (100) crystal on the flank of the low angle side, the centre and the flank of the high angle side of the rocking curve. (*d*), (*e*) Transmission topographs (022 reflection) on the centre and the tail of the low angle side of the rocking curve.

As diamonds are becoming more and more perfect continuous collaboration between crystal growth and characterization is needed.

Acknowledgments

We are grateful to S Goto (SPring-8/JASRI), M Takahashi (SPring-8/JAERI) and H Sumiya (SEI) for their helpful disscusions.

References

Andrews S and Cowley R 1985 *J. Phys. C: Solid State Phys.* **18** 6427
Arthur J *et al* 2002 *Linac Coherent Light Source (LCLS) Conceptual Design Report SLAC-R-593* (Stanford, CA: SLAC)
Bowen D and Tanner B 1998 *High Resolution X-ray Diffractometry and Topography* (London: Taylor and Francis) chapter 7
Brinkmann R, Materlik G, Rossbach J and Wagner A 1997 *Conceptual Design Report of a 500 GeV e^+e^- Linea Collider with Integrated X-ray Laser Facility DESY97-048* (Hamburg: DESY)
Clackson S and Moore M 1989 *Indust. Diamond Rev.* **49** 128
Freund A 1995 *Opt. Eng.* **34** 432
Hoszowska J, Freund A, Boller E, Sellschop J, Level G, Härtwig J, Burns R, Rebak M and Baruchel J 2001 *J. Phys. D: Appl. Phys.* **34** A47
Iida A and Kohra K 1979 *Phys. Status Solidi* a **51** 533
Ishikawa T 1990 *J. Cryst. Growth* **103** 131
Kowalski G, Moore M, Gledhill G and Maričić 1996 *J. Phys. D: Appl. Phys.* **29** 793
Lomov A, Zaumseil P and Winter U 1985 *Acta Crystallogr.* A **41** 223
Lübbert D, Baumbach T, Härtwig J, Boller E and Pernot E 2000 *Nucl. Instrum. Methods* B **160** 521
Moore M, Golshan M, Kowalski G, Reid G, Collins J and Murphy B 1999 *J. Phys. D: Appl. Phys.* **32** A37
Moore M, Waggett R, Wierzchowski W and Makepeace A 1993 *Diamond Relat. Mater.* **2** 115
Nakayama K, Hashizume H, Miyoshi A, Kikuta S and Kohra K 1973 *Z. Naturforsch. Teil* A **28** 632
Shintake T 2004 *AIP Conf. Proc.* **705** 117
Tamasaku K, Tanaka Y, Yabashi M, Yamazaki H, Kawamura N, Suzuki M and Ishikawa T 2001 *Nucl. Instrum. Methods* A **467–468** 686
Tamasaku K 2004 Unpublished
Toda N, Sumiya H, Satoh S and Ishikawa T 1997 *Proc. SPIE* **3151** 329
Wierzchowski W, Moore M, Makepeace A and Yacoot A 1991 *J. Cryst. Growth* **114** 209
Yarnitsky Y, Sellschop J, Rebak M and Bartolucci Luyckx S 1988 *Mater. Sci. Eng.* **A105/106** 565